Accounting for the effect of forest and fragmentation in probabilistic rockfall hazard

Camilla Lanfranconi[1], Paolo Frattini[1], Gianluca Sala[1], Giuseppe Dattola[1], Davide Bertolo[2], Juanjuan Sun[3], Giovanni Battista Crosta[1]

[1] Università degli studi di Milano – Bicocca, DISAT, Dept. of Earth and Environmental Sciences, Milano 20126, Italy
[2] Regione autonoma Valle d'Aosta, Struttura attività geologiche, Quart 11020, Italy
[3] Key Laboratory of Shale Gas and Geoengineering, Institute of Geology and Geophysics, Chinese Academy of Sciences, Beijing 100029, China

Correspondence to: Camilla Lanfranconi (c.lanfranconi2@campus.unimib.it)

Abstract

The presence of trees along the slope and block fragmentation at impact strongly affect rockfall dynamics, and hazard as a consequence. However, these phenomena are rarely simulated explicitly in rockfall studies. We performed rockfall simulations by using the 3D rockfall simulator ~~HY STONE~~Hy-Stone, modelling both the presence of trees and fragmentation through specific algorithms implemented in the code. By comparing these simulations with a more classical approach that attempt to account implicitly for such phenomena in the model parameters, and by using a new ~~probabilistic rockfall hazard analysis~~Probabilistic Rockfall Hazard Analysis (PRHA) method, we were able to quantify the impact of these phenomena on the design of countermeasures and on hazard.

We demonstrate that hazard changes significantly when accounting explicitly for these phenomena, and that a classical implicit approach usually overestimates both the hazard level and the 95th percentile of kinetic energy, leading to an oversizing of mitigation measures.

1. Introduction

Rockfalls are widespread in mountain ranges, coastal cliffs, volcanos, riverbanks, and slope cuts, and threat people, structures and infrastructures, and lifelines (Crosta et al., 2015). Although rockfalls generally have a limited size, they are extremely rapid processes that exhibit high kinetic energies, long runout and damaging capability (Corominas et al., 2017). Rockfall hazard and risk assessment (Corominas et al., 2005; Agliardi et al, 2009; Lari et al, 2014; Wang et al., 2014; De Biagi et al, 2017; Farvacque et al, 2019, 2021; Hantz et al., 2021) and the design of defensive works (Volkwein et al., 2009) require numerical modelling of rockfalls to assess the dynamics of the blocks (i.e., velocity, kinetic energy and bouncing height) and the lateral and longitudinal spreading (Agliardi & Crosta 2003). In Italy, for example, the design of rockfall barriers is based on the use of the 95th percentiles of the blocks' height in flight and their kinetic energy, obtained from numerical models (UNI 11211; Volkwein et al., 2011). Since rockfall dynamics depends on block geometry, slope topography, surficial geology,

vegetation, and some peculiar rockfall behaviours (e.g. dynamic fragmentation), the reliability of analyses and the efficiency of rockfall protections depend on the ~~accuracy of modeling predictions and on the~~ correct account for all ~~relevant methodological issues~~these variables (Crosta et al., 2015). Both the characteristics of the slope (e.g. topography, material properties and presence of forests) and the type of rockfall (e.g. whether it is fragmental) must be taken into account during modelling, because they contribute to the overall extent of rockfall potential and hazard zonation in mountain areas (Frattini et al, 2012). Both these characteristics can modify the trajectories, the extent and the dynamics of the rockfall events, the frequency, and the probability of impact.

Forests provide important protection against rockfall in steep mountain terrain, defending structures and infrastructures (Berger et al. 2002; Dorren et al. 2004a; Perret et al. 2004). Thanks to this nature-based solution, maintenance and installation costs of technical protection measures, such as embankments or nets, are financially bearable or can even be avoided at many places due to the reduction of rockfall rebound heights and impact energies by previous impacts on trees (Grêt-Regamey et al., 2008; Häyhä et al., 2015; Getzner et al., 2017; Moos & Dorren, 2021). Although this protective effect is evident in hazard assessment processes because it supports decisions on risk prevention measures, it is often accounted only in implicit terms, by adopting a set of modified restitution coefficients (Pfeiffer and Bowen 1989; Azzoni et al, 1995). ~~More rarely~~Less frequently, the presence of trees is simulated explicitly by using numerical modelling approaches (Dorren et al. 2006; Stoffel et al. 2006; Berger and Dorren 2007; Bigot et al. 2009; Jancke et al. 2009; Rammer et al. 2010; Leine et al. 2014; Radtke et al. 2014; Kajdiž et al. 2015; Dupire et al. 2016; Moos et al. 2017; Toe et al. 2018).

When stiff and strong rock blocks hit a hard impact substratum or other blocks of comparable size like a talus deposit, they may fragment and explode (Crosta et al., 2015). The rockfall fragmentation process is defined as the separation of the initial rock mass into smaller pieces generally upon the first impact on the ground (Evans & Hungr, 1993), and the resultant fragments propagate downslope following ~~independent~~ trajectories and new dynamics (especially in terms of kinetic energy and height) compared to the source block. This definition covers both the disaggregation of the block fragments delimited by pre-existing ~~fractures~~discontinuities in the initial mass and the generation of new fragments due to the breakage of intact rock (Corominas et al. 2012; Ruiz-Carulla, 2018). Block fragmentation is generally at the origin of extreme behaviors, major damages and accidents, and can interact strongly with protection structures (Nocilla et al., 2009; Wang et al., 2010; Corominas et al., 2019). Even if fragmentation during rockfall is recognized as fundamental in risk analysis (Corominas et al. 2012), a complete understanding of the process during rockfall has not been achieved so far, remaining a phenomenon largely neglected during numerical modelling. Only a few numerical codes allow modelling propagation that explicitly takes into account fragmentation (Crosta et al., 2003; Frattini et al, 2012; Matas et al., 2017; Ruiz-Carulla, 2018). When missing an explicit algorithm, the modeling of rockfalls with fragmentation can be done with two alternative approaches: either the model is calibrated to replicate the spreading of the event, including the most distal fragments, or the model is calibrated to replicate only the main deposit, neglecting the most distal blocks. The first approach leads to hazard overestimation, the second to hazard underestimation.

The aim of this paper is to quantify rockfall hazard when accounting for the presence of trees and fragmentation with an explicit simulation approach (i.e. using specific ~~algorithms~~model), and to evaluate the differences with a classical approach that does not simulate explicitly such phenomena. The simulator Hy-Stone (Crosta et al. 2003; Crosta et al. 2004), which allows to model both the presence of forest and fragmentation, and a new revised Probabilistic Rockfall Hazard Analysis (PRHA) are adopted to quantify the impact of these phenomena on the design of countermeasures and on hazard.

2. Methods

2.1 Rockfall ~~simulations~~analysis

2.1.1 Hy-Stone (HS)

The ~~simulation~~analysis of rockfall propagation was performed by means of Hy-Stone, a 3D rockfall simulator that reproduces the block motion from the dynamics equations (Crosta et al. 2004; Frattini et al. 2012; Dattola et al., 2021) using a triangulated vector topography derived from Digital Terrain Models (DTMs). The model allows to simulate blocks with the shape of spheres, cylinders, ellipsoids, and discs. The stochastic nature of rockfall processes ~~and parameters are~~is accommodated by slope morphology and roughness, and by the random sampling of most parameters from different probability density distributions (e.g. uniform, normal, exponential). The block trajectories are computed by splitting them in a succession of elementary motions: free fly, rolling, sliding and impacts/bouncing. When the impact process is concerned, Hy-Stone has many different models comprising the constant and not-constant restitution coefficients (Pfeiffer and Bowen 1989) and the ~~evolution of the~~ elasto-visco-plastic model initially ~~proposed~~formulated by di Prisco and Vecchiotti (2006) and ~~further~~subsequently extended ~~to~~by introducing rotation and prismatic blocks (Dattola et al., 2021). Specific sub-model ~~components~~ explicitly account for the interactions between blocks and countermeasures or structures, between blocks and trees, and fragmentation (Frattini et al. 2012).

2.1.2 Tree-impact ~~algorithm~~sub-model

The block-forest interaction is modeled through a stochastic tree-impact ~~algorithm. Trees~~sub-model. Tree height, trunk diameter, absorbable energy, and density (as number of trees ~~in~~per 10 square meters ~~square~~) are used ~~by the algorithm~~as input to calculate at each cell a probability of impact, that depends on the tree density, tree size and block size, and, in case of impact ~~of impact~~, a loss of block kinetic energy and a lateral deviation of the trajectories (Frattini et al., 2012) are ~~considered~~computed. The block kinetic energy lost by impact on tree stems is greatest for central impacts, and decreases according to a Gaussian distribution away from the stem axis, while the angular deflection of the block on impact is assumed to vary according to the type of impact (central, lateral, scour) (Dorren et al 2004b).

2.1.3   Fragmentation algorithmsub-model

Hy-Stone can simulate the splitting up of a block in fragments moving independently from each other. The fragmentation occurs at impact when the kinetic energy of a block exceeds a thresholdlimit energy defined by the relationship elaborated by Yashima et al, (1987).) based on the Weibull distribution. The Yashima expression is:

$$E_{k,lim} = 0.15 \, B_f \, C_f \left(\frac{1-v^2}{E}\right)^{\frac{2}{3}} (2R^{bl})^{\frac{3m_w-5}{m_w}} \left[\sigma_0 V_0^{1/m_w}\right]^{5/3} \tag{1}$$

where $E_{k,lim}$ is the limit energy, v is the Poisson's coefficient, E is the Young's modulus, R^{bl} is the radius of the parent block, V_0 is a reference volume, σ_0 is the strength at the reference volume and m_w is the Weibull distribution parameter. Coefficients B_f and C_f are computed according to the following expression:

$$B_f = \begin{cases} 1.0 \; if \; m_w = 1 \\ \frac{\pi}{A_f} \; otherwise \end{cases} \tag{2}$$

and

$$C_f = 6^{\frac{5}{3m_w}} \tag{3}$$

Coefficient A_f is the result of the following expression:

$$A_f = \begin{cases} 0 \qquad\quad if \; m_w = 1 \\ \frac{5(m_w-1)}{3m_w} \; otherwise \end{cases} \tag{4}$$

Therefore, the threshold fragmentation energy depends on the geomechanical properties of the block and its volume (the larger the block, the lower the fragmentation energy). Once the fragmentation criterion is satisfied, a distribution of fragments is generated with a size determined according to a power-law distribution.:

$$R(D) = \left(\frac{D}{D_m}\right)^n \tag{5}$$

where $R(D)$ is the fragment size distribution, D is the fragment diameter, D_m is the maximum fragment diameter and n is a model parameter. The maximum fragment size is a fixed fraction of the parent block size. The number of fragments is computed according to athe mass conservation criterion(the total fragments mass must be about the mass of the parent block) and the above distribution, and the energy of each fragment is calculated assuming thatby means of the following expression:

$$E_{f,i}^{k,tr} = \beta\left(m_{fi}\right)^{\alpha_f} \tag{6}$$

in which m_{fi} is fragment mass, $E_{f,i}^{k,tr}$ is the translational kinetic energy available after impact is equally distributed among all fragments. Fragment projection velocity and direction are thenof the fragment and α_f is a model parameter. β is computed

~~according to~~by imposing the translational energy conservation ~~criteria. Results show~~. Once the kinetic energy of fragment is known the inverse formula gives the fragment ejection velocity modulus. Fragment ejection velocity direction is computed stochastically within a cone whose aperture is a model parameter. Frattini et al. (2012) showed that block fragmentation has an effect on the runout extent and on the spatial distribution of velocities and heights of the flying rocks. The largest fragments, however, display a ~~behavior~~behaviour that is more similar to that of the parent blocks.

2.2 Rockfall hazard assessment

To assess rockfall hazard, we propose a new revised PRHA (Probabilistic Rockfall Hazard Analysis), based on Lari et al. (2014), to build rockfall hazard curves starting from a set of block-volume scenario simulations. This methodology owes its idea on Cornell's (1968) probabilistic seismic hazard analysis (PSHA), which considers all possible earthquake scenarios to provide the exceedance probability of a certain level of ground motion at a site within a defined time frame. For each block-volume scenario, s, the probability of exceeding a certain value of intensity (i~,~.e. the reach of a specific value of kinetic energy), for each position along the slope (z) is:

$$P(I > i) = \int_{I_c}^{\infty} p(I)dI \qquad (1)$$

$$P_s(E_k > \bar{E}_k) = \int_{I_c}^{\infty} p_s(E_k)dE_k \qquad\qquad\qquad\qquad (7)$$

where ~~p(I)~~$p_s(E_k)$ is the probability density function of kinetic energy at the position z~.~ for the scenario s. Multiplying the exceedance probability by the annual frequency of occurrence (~~f,~~f_s), we obtain the annual rate at which i is exceeded, ~~F(I>i)~~$F_s(E_k > \bar{E}_k)$ as:

$$F(I > i) = f \cdot P(I > i) \qquad (2)$$

$$F_s(E_k > \bar{E}_k) = f_s \cdot P_s(E_k > \bar{E}_k) \qquad\qquad\qquad\qquad (8)$$

The annual frequency of occurrence (~~f,~~f_s) of each scenario combines the onset frequency (~~f₀,~~f_o) and the transit frequency (~~ft,~~$f_{t,s}$) at a certain position and for the specific scenario:

$$f = f_0 \cdot f_t \qquad (4)$$

$$f_s = f_{0,s} \cdot f_{t,s} \qquad\qquad\qquad\qquad (9)$$

The onset frequency (~~f₀,~~$f_{o,s}$) of blocks with a certain volume, ~~V,~~V_s, can be expressed in terms of magnitude—frequency relationships (Hungr et al. 1999; Dussauge et al. 2003; Rosser et al., 2007).

$$F = N(V) = aV^{-b} \qquad\qquad (5)$$

$$f_{0,s} = N(V_s) = aV_s^{-b} \qquad\qquad\qquad\qquad\qquad\qquad\qquad\qquad (10)$$

where $N(V)(V_s)$ is the cumulative number of individual blocks with volume larger than $V; V_s$ for the scenarios s; parameter a depends on both the area extent and the overall susceptibility of the cliff, whereas the power law exponent, b, mainly depends on lithology and geological structure (Hungr et al., 1999). To properly account for the frequency of individual blocks that propagate on the slope, it is necessary to combine the volume frequency relationship of rockfall events with the volume frequency relationship of blocks (Hantz et al., 2018; Hantz et al., 2020). The first relationship can be developed from surveyed historical events (e.g. Dussauge-Peisser et al. 2002; Chau et al., 2003; Guzzetti et al., 2003; Guthrie and Evans, 2004; Malamud et al., 2004) and provides annual frequencies of released rockfall volumes. However, these volumes should not be used for hazard analysis because single rockfall events disaggregate or fragment (Ruiz-Carulla et al., 2017) soon after the detachment and during propagation into a distribution of smaller individual blocks. On the other hand, the volume frequency relationship of blocks can be derived from the rock mass fracture network or directly from already stopped blocks, both in the talus (Ruiz-Carulla et al., 2017), along roads (Hungr et al. 1999), and caught by rockfall nets within a certain range of time (Matasci et al., 2015; Moos et al., 2018). However, these distributions usually lack the temporal frame that allows to correctly estimate the annual frequency. The combination of the two distributions can be achieved by calculating the total volume of the event (integrating the first distribution) and by calculating the a parameter of the second distribution by assuming the total volume to be equal to the first one (Hantz et al., 2018).

The transit relative frequency (f_t) can be calculated for the rockfall simulation and corresponds to the ratio between the number of potential paths passing through a position ($t)t_s$) and the total number of simulated paths from the rockfall trajectories, (t_{tot}):

$$f_t = \left(\frac{t}{t_{tot}}\right) \qquad\qquad\qquad (6)$$

$$\text{by } f_{t,s} = \left(\frac{t_s}{t_{tot}}\right) \qquad\qquad\qquad\qquad\qquad\qquad\qquad\qquad (11)$$

For rockfall scenarios with different magnitude that occur in a certain position along the slope, the total annual rate at which i is exceeded, $F_{tot}(E_k > \bar{E}_k)$, derives from the sum of these scenarios, s:

$$F_{tot}(E_k > \bar{E}_k) = \sum_{s=1}^{N} F_s(E_k > \bar{E}_k) = \sum_{s=1}^{N} f_s P_s(E_k > \bar{E}_k) \qquad\qquad\qquad (12)$$

By assuming a homogeneous, stationary Poisson process for the occurrence of the events (Crovelli, 2000), the probability of exceeding each intensity i in the next $T \; T$ years from this annual rate, $P_{poiss}; P_{poiss1}$ is:

$$P_{\substack{poiss}}(I > i, T) = 1 - e^{-F_{tot}T} \qquad (8)$$

175 $\quad P_{poiss}(E_k > \bar{E}_k i, T) = 1 - e^{-F_{tot}\,T}$ _______________________________________ (13)

This represents the hazard curve at each position along the slope.

With respect to Lari et al. (2014), the revised PRHA method adopts a more flexible non-parametric approach for the kinetic energy probability distribution. Moreover, the new PRHA implements the approach proposed by Hantz et al (2016, 2019) for the calculation of the onset frequency (f_o), f_o), using the frequency-size distribution of the blocks observed along the talus to

180 downscale the magnitude-frequency distribution of larger study areas.

2.3 Demonstration case studies

The application of potential rockfall scenarios was performed at the two representative sites that were recently affected by rockfall events in the Aosta Valley Region (Western Italian Alps) showing a significant role of forest and fragmentation at

185 Saint Oyen and Roisan (Figure 1), respectively. During both the events, the rockfalls impacted roads and buildings, thus requiring a practical implementation of hazard assessment (for zonation) and the design of protection barriers (for mitigation). Saint Oyen and Roisan are located in the Western Alps, within the Austroalpine-Pennidic collisional prism, consisting of overburden layers formed by continental crust and fragments of oceanic lithosphere, strongly reworked by the Alpine tectono-metamorphic processes (Dal Piaz et al., 2016).

190 In the Saint Oyen case study (45°48'59.0"N 7°12'21.0"E), about 17,500 m³ of Ruitor micascists detached in March 2020, and reached a service road and the playing field in the lower part of the slope, passing through a mature fir forest. The presence of the forest significantly influenced the blocks distribution along the slope, increasing the lateral dispersion of trajectories and reducing their mobility. The case study is well documented by UAV flights conducted by the Regional Authority soon after the events, allowing for a detailed mapping of arrested blocks on the slope. We adopted this case study to investigate the role

195 of forest, which has been fundamental for the rockfall dynamic, as observed in the field. Although minor fragmentation may have occurred during the event, we neglected it during the simulation to focus on tree-impact only.

Less than 10 km far, at Roisan (45°47'49.3"N 7°18'49.0"E), about 1,050 m³ of Arolla gneiss toppled in October 2019 and impacted after 20 m of free fall (Polino et al., 2015) against a bench. While the main body of the rockfall stopped in a relatively flat area close to the source area, two blocks reached the foot of the slope causing the interruption of a municipal road. The

200 event is documented by a post-event UAV flight, and by a detailed field survey of the blocks. For this case study, the presence of forest was minor due to the size and age of the trees and it has been neglected in order to reveal better the role of fragmentation.

3. Analysis and results

For both case studies, we firstly back-calibrated the model parameters on the rockfall events in order to simulate several volume
scenarios from local-scale rockfall source areas (with and without the use of specific algorithms for tree-impact and fragmentation) to quantify the differences in terms of dynamics, spreading and rockfall hazard. We simulated ~~both~~ all the scenarios by using spherical blocks and a 3D topography derived from the available 1 x 1 m Lidar DTM of Aosta Valley Region. The characteristics of each simulation, the number of simulated blocks, and the parameters adopted when using the two algorithms are reported in supplementary Table S1, 2 and 3.

3.1 Calibration by back-analysis

The calibration of model parameters was obtained by fitting the longitudinal and lateral extent of rockfall ~~events~~trajectories and deposits by using the Hy-Stone model with and without tree-impact and fragmentation. In particular, we simulated the following scenarios (Figure 1):

- SO_HS (Saint-Oyen tree impact implicit): the values of parameters are ~~modified~~set to account for the forest, e.g. increasing rolling friction and reducing the tangential restitution coefficient. This is the most classical approach adopted in the practice to "simulate" the effect of forest with an implicit approach.
- SO_HS$_{tree}$ (Saint-Oyen tree impact explicit): the values of parameters are calibrated by adopting the Hy-Stone tree-impact algorithm that explicitly simulates the effect of forest; in this case, the motion parameters used in the simulation do not account for the forest.
- R_HS (Roisan Fragmentation Implicit): the values of parameters are ~~modified~~set to allow the model to replicate the spreading of the event, including the most distal blocks, implicitly accounting for the possibility of fragmentation.
- R_HS$_{frag}$ (Roisan Fragmentation Explicit): the values of parameters are calibrated by adopting the Hy-Stone fragmentation algorithm that explicitly simulates the distal blocks as fragments.

For Roisan, we experimented a different calibration strategy that replicates the spreading of the main deposit only (R_HS$_{short}$), neglecting most distal blocks (Figure 1E). Although this strategy is physically correct to simulate non-fragmenting blocks, it provides an overall spreading that strongly underestimate the possible reach distance of fragments and the hazard level, accordingly.

For Saint-Oyen, both the simulations (~~R~~SO_HS, ~~R~~SO_HS$_{tree}$) provide a good match with the main deposit of the 2020 event (Figure 1 A and B), with a slightly larger spreading when using the tree-impact algorithm, consistently with the fact that the impact with trees adds a component of lateral dispersion to the trajectories.

For Roisan, we can observe a good match between the longitudinal and lateral extent of the main deposit from the 2019 event and the simulations (R_HS, R_HS$_{frag}$) but we observe an overestimation of the blocks reaching the paved road (18 blocks modelled, while just 2 blocks during the event) when the fragmentation algorithm is not used (Figure ~~1A~~1C). The comparison with simulated stopping points shows that the model without fragmentation is able to reach the maximum distance, but not in

the right location, since trajectories are strongly controlled by topography. This does not happen with the fragmentation algorithm, which is able to replicate the right position of the distal blocks in the meadow (Figure 1B).1D).

In addition, the volume distribution is also considered. To this purpose the In-situ Block Size Distribution (IBSD) at the cliff considered in the previous numerical simulations was obtained previously by the Geological survey of Valle d'Aosta by means of a terrestrial laser scanner survey. In the Figure S1 a comparison of the Rock Block Size Distribution (RBSD) obtained with the ortophotos at the toe of the slope, and the distributions obtained with the scenario R_HS, R_HS$_{frag}$ is shown. The comparison reveals a good agreement since the curves are parallel each other although the Hy-Stone distributions overestimate the in situ one.

Table 1 Table 2and Table 2 report the values of normal and tangential restitution coefficients and of the friction coefficient for the different slope materials used in the rockfall numerical simulations, in the cases of SO_HS and supplementaryR_HS. Supplementary Table S1 and Table S2 report the parameters of tree-impact and fragmentation algorithms. used in the cases of SO_HS$_{tree}$ and R_HS$_{frag}$.

3.2 Effect of tree-impact and fragmentation algorithmsub-models on kinetic energy

To quantify the effect of explicitly simulating tree-impact and fragmentation in rockfall modelling, we performed simulations for five volume scenarios in which the released volumes are changed (Table 3), using the modelingmodelling parameters that were back-calibrated from the events as previously described. The volume scenarios range from 0.001 m^3 to 100 m^3 to encompass the block sizes surveyed on the field at the two sites.

For the spatial analysis, we divided the slope into a 10 x 10 meters square lattice and we calculated statistics of kinetic energy within each square.

3.2.1 Effect of tree-impact algorithmsub-model

Figure 2Figure 2 shows the 95th percentile of the blocks kinetic energy in each 10 m square. considering the first and fifth scenario with and without the forest sub-model. This statistic variable has been chosen since it is frequently used for designing defensive works (UNI 11211; Maciotta et al., 2015; Lambert et al., 2021). In the case of small volume blocks, the simulation without tree-impact algorithmsub-model (Figure 2a2A) shows a central sector characterized by the highest kinetic energies (from 2,500 kJ up to over 10,000 kJ for the 95th percentile), and a distal zone characterized by lower values. Trajectories are able to reach the base of the slope, the unpaved road, buildings, and playing field, and overpass the location of the outermost blocks of the 2020 event. When using the tree-impact algorithmsub-model (Figure 2B) the number of trajectories passing through the central sector of the slope decreases dramatically. The trajectories that reach the base of the slope are concentrated in the area affected by the 2020 event where the forest is damaged. These trajectories reach only the unpaved road, with associated 95th percentile kinetic energy values of less than 2,500 J. For large blocks (Figure 2 C and Dfifth scenario), the

kinetic energy is high enough to nullify the effect of forest, and the two ~~scenarios~~analysis without and with tree-impact ~~algorithm~~sub-models become similar~~.~~ (Figure 2 C and D).

270 From these results, it is evident that the use of the tree impact ~~algorithm~~sub-model is relevant in the case of small volume blocks, for which the simulated trees are able to interrupt most of the computed trajectories, and in any case to decrease the kinetic energies. On the contrary, tree-impact ~~simulation~~analysis is almost irrelevant for large-volume blocks.

~~Analyzing~~Analysing the distribution of kinetic energies along the road and the blocks number at the foot of the slope without (HS) and with (HS_{tree}) the tree impact ~~algorithm~~sub-model, we systematically observe lower values of energy for the HS

275 ~~models~~analyses (Figure 3). ~~In~~Indeed, in these models, the effect of the forest is simulated by ~~modifying~~reducing the restitution ~~and friction~~ coefficients and increasing friction coefficient, calibrated on the range of kinetic energies of the event. However, this coefficients modification is independent of the ~~kinetic energies~~block mass of the simulated blocks, and, therefore, it is not possible to observe the scale effect revealed in the HS_{tree} analyses.

When the kinetic energies are lower both than the calibrated kinetic energies and the kinetic absorption energies of the trees

280 (scenarios S1 and S2), the classical HS approach overestimates the runout (see the large number of blocks intersecting the road after crossing the forest in Figure 2 A). Instead, the HS_{tree} algorithm intercepts, slows, and stops the least energetic blocks, allowing only the most energetic to reach the lower part of the slope. As a result, few transits are obtained, but with much higher kinetic energies due to the filtering effect of the forest (Figure 3).

~~When~~In contrast, when the kinetic energies grow beyond the calibration range (scenarios S4 and S5), the classical HS approach

285 continues to apply the forest effect (through the modified parameters) even though the kinetic energies are well above the tree absorption energies, underestimating the runout (the number of blocks intercepting the road remains about the same as in the low energy scenarios) and the kinetic energies (Figure 3). ~~In contrast,~~For the HS_{tree} ~~algorithm~~analyses in these scenarios S4 through S5, ~~shows~~show higher kinetic energies and a high number of transits (compared to the lower-volume scenarios) because the effect of the trees becomes negligible, as it should be (Figure 3).

290 In the intermediate S3 scenario, greater congruence between the two approaches HS and HS_{tree} is observed (Figure 3) because the simulated volumes are ~~more coincident with~~similar to the calibration range (between 0.001 m^3 and 34 m^3).

3.2.2 Effect of fragmentation ~~algorithm~~sub-model

Figure 4 shows the 95th percentile of the blocks kinetic energy in each 10 m square grid with and without the adoption of the

295 fragmentation ~~algorithm.~~sub-model considering the first and fifth scenarios. The ~~behavior~~behaviour of the ~~models~~analyses with small or large block volumes is extremely different. In the case of small volume blocks, the adoption of fragmentation algorithm is almost negligible, because blocks are too small to undergo fragmentation. In Figure 4 A the highest 95th percentile values of kinetic energy for the first scenario and without fragmentation are concentrated in the area located just below the modelled source and at the highest escarpment, and only four trajectories characterized by values up to 3 kJ reach and cross

300 the paved road. In Figure 4 B we observe that the highest 95th percentile values considering the fragmentation are concentrated

in the area close to the ~~wall~~cliff, but only one trajectory passes the road, characterized by 95th percentile of kinetic energy much lower (up to 1.5 kJ).

For larger blocks (S5 scenario), the difference with and without fragmentation is much more significant because more ~~than half of the~~ blocks are fragmented (612 out of 2646, 23%). In Figure 4C without fragmentation the runout achieved by blocks does not exceed that of Figure ~~4a~~4A, but with much larger values associated with the 95th percentile of kinetic energy reached all over the slope. The area located just below the modelled source and in the highest escarpment is characterized by kinetic energy values greater than 50,000 kJ at the intersection with the unpaved road. Values remain high also at the intersection with the paved road. In Figure 4D in which the fragmentation is considered there is an increase in the number of blocks crossing the roads, a consequent spread of trajectories with longer runouts (more than those actually achieved during the event) and a decrease in kinetic energy due to block fragmentation. On the unpaved road, the values associated with the 95th percentile drop to 50,000 kJ, and where the event boulder stopped it decreases to 8,000 kJ. At the intersection with the paved road, percentile values are more frequently lower than 15,000 kJ except in an isolated section where they reach 50,000 kJ and over.

~~Analyzing~~Analysing the distribution of ~~Kinetic Energies~~kinetic energies along the paved road at the foot of the slope without (HS) and with (HS$_{frag}$) the fragmentation ~~algorithm~~sub-model, we systematically observe higher values of energy for the HS ~~models~~analyses (Figure 5). Although during the event very few blocks crossed the paved road and only two of them reached the meadow at the foot of the slope, the calibration of the model without fragmentation was accomplished by adjusting the parameters in order to reach the maximum runout. This causes a strong overestimation of the number of blocks crossing the paved road, a general overestimation of the landslide runout, and therefore also an overestimation of the kinetic energies at the element at risk. As already said for the Saint-Oyen case study, the runout in the HS models is almost independent from the ~~kinetic energy of the blocks.~~block mass. Therefore, the number of transits is roughly constant in all ~~six~~five scenarios.

~~In~~Instead, in the HS$_{frag}$ approach, the kinetic energy at the element at risk is systematically lower because the model is calibrated in order to allow only ~~trajected~~ejected fragments (characterized by much lower volumes with respect to original blocks) to reach and cross the paved road as occurred during the event. The number of fragments reaching the road increases significantly through different volumes scenarios (from S1 to S5). This depends on the relationship between block size and fracture energy (Yashima et al., 1987); according to this relationship, the fracture energy scales with the radius of the block by an exponent that depends on the Weibull's coefficient of uniformity, and is always lower than 3, which is the scaling of the kinetic energy with radius. Hence, the larger the block, the higher is the probability of fracturing for a certain velocity.

The two approaches HS and HS$_{frag}$ provide similar results in the S4 scenario (characterized by simulated volumes that are ~~more coincident with~~similar to the calibration range, between 0.5 m^3 and 23 m^3) both in terms of number of blocks intersecting the road and in terms of kinetic energies: compared to all other scenarios, less than an order of magnitude separates the two 95th percentile values of kinetic energy.

3.3 Rockfall Hazard

335 ~~The~~As explained in the metholody section, the assessment of rockfall hazard requires the onset frequencies $f_0$$f_{0,s}$ for each magnitude scenario, the transit frequency, $f_t$$f_{t,s}$ and the distribution of kinetic energy in each position along the slope.

For the calibration of onset frequency parameters (eq. ~~5),~~10), we adopted the methodology of Hantz et al (2018) ~~to obtain the frequency distribution of blocks for different volume classes, by combining~~who related the magnitude–-frequency relationship of all rockfall events within a fixed site with the size–-frequency relationship of blocks along the talus. ~~The first was~~ for a

340 specific event in the same site.

We obtained magnitude-frequency relationship by ~~analyzing~~analysing the available rockfall database of the Valle d'Aosta region, which includes 306 events with volume information (Figure 6). Among them, only 25 belongs to the same catchment of the case studies (Buthier catchment, Figure 6). ~~This~~Since this subsample appears to be insufficient to characterize the magnitude–-frequency curve, especially for smaller volumes~~, and~~ that are not recorded, we therefore adopted the entire

345 inventory that we fitted with a maximum likelihood approach, obtaining a good power-law fitting ($R^2 = 0.99$) for rockfalls larger than 10 m³, with a scaling exponent of 0.56. We believe that this parameter value is reliable also for the Buthier catchment, since the fitting curve has the same slope of larger rockfalls volumes (with a volume greater than 500 m³) within the subsample. ~~The~~Therefore, this parameter b is adopted for the two cases studies.

For the parameter a, we used the size–-frequency relationship of blocks along the talus ~~was~~obtained by image analysis ~~only~~

350 ~~for Saint-Oyen due to a larger number of blocks and a better quality of the imagery~~. Figure 7 shows an excellent power-law fitting ($R^2 = 0.99$) for blocks larger than 0.2 m³, with a scaling exponent b equals to 1.22. Eventually, by ~~combining~~relating the ~~two distributions~~magnitude-frequency size-frequency and accounting for the potential unstable area of both case studies, we obtained an a value of 0.0072 and of 0.0021 for Saint-Oyen and Roisan, respectively. The resulting onset frequencies for the different volume scenarios are reported in Table 3 for both case studies.

355 Both transit frequency (f_t)$f_{t,s}$) and the distribution of the kinetic energy come from the rockfall simulation trajectories sampled within 10x10 m cells. In order to characterize the kinetic energy distribution, we tested the hypothesis adopted by Lari et al, (2014), who assumed the logarithm of the kinetic energy to be normally distributed, and obtained the kinetic energy probability density ~~p(I)~~$p_s(E_k)$ by using the mean and standard deviation statistics. The Kolmogorov-Smirnov's test (Figure 8) shows that the normality is not rejected for more than 50% of the 10x10 m cells when using Hy-Stone without additional algorithms.

360 However, this percentage is lower when using the tree-impact and fragmentation algorithms, suggesting that a non-parametric approach should be adopted when the level of complexity increases.

By combining the various scenarios and taking into account their associated probabilities~~,~~ (Equation 12), we constructed the hazard curves (by equation ~~8),~~13), which show the probability of exceeding a certain level of intensity in 50 years.

Figure 9 Example of hazard curves characterized by a non-logarithmic trend, calculated in five cells of R_HS model.

365 Figure 9 shows hazard curves only for some representative cells. We can assert that ~~hazard curves~~they do not always have a logarithmic distribution, and that some curves (not here reported) do not reach the exceedance probability of 0.1 due to a very

low transit frequency. ~~Then~~Subsequently, for each location along the slope and for each model ~~run~~analyses (SO_HS, SO_HS$_{tree}$, R_HS, and R_HS$_{frag}$), we ~~reduced~~computed from each hazard curve ~~to a single value in order to represent~~, fixing the ~~hazard through a hazard map. As~~exceedance probability in 50 years at 10% as done by Lari et al (2014), ~~we chose~~ the corresponding kinetic energy ~~with a 10% chance of being exceeded in 50 years, and we extracted this value from each hazard curve.~~which is used to represent the hazard through a hazard map (Figure 10).

Compared to the SO_HS model~~,~~ (Figure 10A), in SO_HS$_{tree}$ (Figure 10B) the hazard decreases because kinetic energy is significantly lowered, except in correspondence of the two sectors most affected by the event (see calibration in ~~Figure 1)~~Figure 1) where it remains similar ~~(Figure 10~~(Figure 10 A and B). The total area involved remains about the same, although with slightly lower runout. However, if only the areas with ~~Ek>1 kJ~~$Ek > 1kJ$ are considered, hazard decreases significantly along the road at the foot of the slope.

For the Roisan case study, compared to the R_HS model, in R_HS$_{frag}$ the hazard decreases because the kinetic energy is significantly lowered, but note that the area involved increases ~~(Figure 10~~(Figure 10C and D). Analysing the distribution of the hazard values ~~(Figure 11)~~(Figure 11) at the foot of the slope obtained by the different approaches without and with the tree impact and fragmentation algorithms, we observe an overestimation of the potential hazard in both case studies. In the Roisan case study, the overestimation is particularly high because the chance to fragment the blocks into smaller fragments greatly reduces the kinetic energy of those. Moreover, the distribution is less sparse because the only blocks with an energy value higher than the minimum energy value (1 kJ) that are able to reach the foot of the slope are few and localized in a 10-meter corridor.

4   Discussion

When hazard and risk need to be assessed, it is required to have a repeatable procedure and possibly a unique result. This study demonstrates that different modelling approach can influence both the ~~final result of~~ hazard analysis and ~~risk mitigation~~the design of countermeasures, but also points out the problems involved in advanced modelling, leading to necessary discussions on the topic.

4.1 Tree impact

The classical approach for modelling rockfall propagating along forested slopes is based on the modification of restitution and friction coefficients, calibrated on the extent of block propagation. This study shows that the adoption of this set of modified restitution coefficients provides a correct replication of the maximum lateral spreading and longitudinal runout, but inaccurate ~~dynamic~~energy of blocks. In fact, the modification of the restitution coefficients is independent on the size of the blocks and can slow down even those blocks that are large enough to be actually unaffected by the presence of the forest. This leads to an overestimation of rockfall runout and of the number of blocks reaching the elements at risk. When the protective role played by the forest is explicitly simulated (HS$_{tree}$), the hazard decreases due to the forest protection, but the high-percentiles of kinetic

energy become higher. This occurs because the trees ~~intercept~~stop the blocks with lower kinetic energy, ~~with~~generating a

400 *filtering effect* of the larger blocks, leading to the risk of considering, paradoxically, the presence of the forest as more dangerous. These considerations open an important discussion on the opportunity to design the defensive works only based on percentiles of the kinetic energy.

4.2 Fragmentation

405 In case of rockfalls charcaterized by ~~dynamic~~ fragmentation, the classical approach for calibrating the model with this events is based on a conservative adjustment of the parameters in order to reach the maximum runout of single fragments. We demonstrate that this approach leads to a strong overestimation of the number of transits (Figure 4), the overall landslide runout, the kinetic energy of blocks impacting the elements at risk ~~(Figure 5),~~(*Figure 5*), and the hazard ~~(Figure 10).~~(Figure 10). On the other side, the alternative approach to replicate only the main deposit, neglecting the most distal blocks would

410 result in an underestimation of all these quantities (supplementary Figure S5). Therefore, regardless of whether deciding to simulate only the blocks that have stopped in the main deposit ~~(Figure 1E~~(Figure 1E) or to extend the trajectories to the maximum fragment extent ~~(Figure 1C~~(Figure 1C), this study demonstrates that the result is fundamentally incorrect, especially for the design of defensive works. On the other side, the explicit modelling of fragmentation is still challenging from both a theoretical point of view (Ruiz-Carulla et al., 2017; Shen et al., 2017; Guccione et al., 2022) and a practical point of view, due

415 to the difficulty to calibrate the geotechnical parameters that control fragmentation. This adds further uncertainty in the analysis of rockfall dynamics and hazard.

~~From the~~The results of hazard computation ~~with and without~~ when using the fragmentation ~~algorithm, which~~ show a decrease of the hazard ~~decreases~~. However, as in case of forest, this results from the fact that more ~~weight~~importance is given to the kinetic energy of the blocks and not the frequency. Is it correct to infer that the hazard decreases, mostly due to the decrease

420 of kinetic energy, even if the frequency increases, ~~the kinetic energy of the blocks decreases, but~~ and the trajectories are much more dispersed ~~much more? We believe~~ ? Our belief is that ~~it~~this inference is not ~~completely correct because at spatial level, more zones are involved~~entirely accurate since the area affected by rockfalls is larger, even if ~~from~~blocks are smaller ~~blocks~~. This discussion leaves room for future new studies.

4.3 Probabilistic rockfall hazard

425 The PRHA approach allows to quantify rockfall hazard in terms of hazard curves, thus describing the probability of exceeding a certain level of hazard. For each magnitude scenario, the approach overcomes the need of selecting a statistic of the kinetic energy at a certain positon along the slope (Agliardi et al, 2009; Farvacque et al, 2021), and allows to consider the full energy distribution within a certain grid cell. With respect to Lari et al. (2014), the revised PRHA method presents two improvements:

430 (i) ~~it adopts~~the adoption a more flexible non-parametric approach for the kinetic energy probability distribution, instead of assuming a log-normal distribution, that we demonstrate in this paper to be frequently violated if tree impacts and fragmentation ~~exist~~subsist (Figure 8); (ii) ~~it implements~~the implementation of the approach proposed by Hantz et al (2016,

2019) for the calculation of the onset frequency (f_o) $f_{o,s}$). This approach allows to ~~combine~~relate the onset frequency estimated from historical catalogues with the frequency--size distribution of blocks along the slope. In fact, the large volumes recorded in the catalogues typically disaggregate into a population of blocks, as soon as they impact on the slope. This disaggregation occurs due to the presence of pre-existing joints and fractures of a jointed rock mass (Ruiz-Carulla et al., 2017) and does not correspond to a ~~dynamic~~ fragmentation. The adoption of the Hantz et al (2016, 2019) approach place emphasis on the block size distribution along the slope, both to define the design volumes (Melzner et al, 2020), and to support the correct definition of the onset frequency.

5 Conclusions

The insight drawn from this study leads us to the conclusions that:

- If we do not explicitly simulate forest, we underestimate the protective role of trees and we consequently overestimate the hazard. On the other hand, the 95th percentile of the simulated kinetic energy of the blocks is higher when adopting the tree-impact algorithm because of the filtering effect performed by trees.
- If we do not explicitly simulate the fragmentation phenomenon, we overestimate the hazard in terms of energy values, but we underestimate the spreading of blocks during the events. The 95th percentile of kinetic energy along the element at risk is significantly lower when adopting the fragmentation algorithm.
- We obtained non-log-normal distributions of the kinetic energy values, so we adopted a non-parametric approach that we demonstrate being suitable for the hazard analysis. We highlight how PRHA fits different methodological models, and we quantify how much explicitly simulating both the interaction with forest and the fragmentation process lead to more accurate hazard mapping.
- As already mentioned in the discussion, we pointed the need to simulate a distribution of blocks that is representative of what already occurred as the so far most likely, because the dimensioning of the mitigation works is centered on the expected and simulated kinetic energies of the blocks. We also used the frequency-size distribution of the blocks along the talus to downscale the magnitude-frequency distribution of the study area, as proposed by Hantz et al (2018), to simulate different volume class scenarios.
- This study highlights the strong dependency of the 95th percentile of kinetic energy on the adopted modelling approach, showing the fluctuations of this value and thus the uncertainty related to the use of this parameter for hazard analysis.

6 Acknowledgments

The authors would like to acknowledge the support of the Geological Survey of the Aosta Valley Region, and also Serena Lari for useful discussions.

7   Data availability

465   The digital elevation model are publicly accessible at https://geoportale.regione.vda.it/download/dtm/ (Geoportale Regione Valle d'Aosta). The numerical simulations results are available from the first or corresponding author upon request.

8   Author contribution

470   CL, PF and GBC contributed to the conceptualisation of the project, formal analysis, investigation, methodology, visualisation, writing of the original draft, and reviewing and editing of the text. DB contributed by data collection with the Geological Survey of the Aosta Valley Region. GS, GD and JS contributed to the analysis, reviewing, and editing of the text.

475 ## 9   Competing interests

The authors declare that they have no conflict of interest.

10 References

Agliardi, F., Crosta, G. B., & Frattini, P. (2009). Integrating rockfall risk assessment and countermeasure design by 3D modelling techniques. *Natural Hazards and Earth System Sciences*, *9*(4), 1059-1073.

480   Azzoni, A., La Barbera, G., & Zaninetti, A. (1995, October). Analysis and prediction of rockfalls using a mathematical model. In *International journal of rock mechanics and mining sciences & geomechanics abstracts* (Vol. 32, No. 7, pp. 709-724). Pergamon.

Berger, F. and Dorren, L. K.: Principles of the tool Rockfor.net for quantifying the rockfall hazard below a protection forest, Schweizerische Zeitschrift fur Forstwesen, 158, 157–165, doi:10.3188/szf.2007.0157, 2007

485   Berger, F., Quetel, C., & Dorren, L. K. (2002). Forest: a natural protection mean against rockfalls, but with which efficiency. In *International congress INTERPRAEVENT* (Vol. 2, pp. 815-826).

Bigot, C., Dorren, L. K., & Berger, F. (2009). Quantifying the protective function of a forest against rockfall for past, present and future scenarios using two modelling approaches. *Natural hazards*, *49*(1), 99-111.

Chau, K. T., Wong, R. H. C., Liu, J., & Lee, C. F. (2003). Rockfall hazard analysis for Hong Kong based on rockfall

490   inventory. *Rock Mechanics and Rock Engineering*, *36*(5), 383-408.

Corominas J, Mavrouli O, Santana D, Moya J (2012) Simplified approach for obtaining the block volume distribution of fragmental rockfalls. In: Eberhardt E, Froese C, Turner AK, Leroueil S (eds) Landslides and engineered slopes, 2, pp 1159–1164.

Corominas, J., Copons, R., Moya, J., Vilaplana, J. M., Altimir, J., & Amigó, J. (2005). Quantitative assessment of the residual

495   risk in a rockfall protected area. *Landslides*, *2*(4), 343-357.

Corominas, J., Matas, G., & Ruiz-Carulla, R. (2019). Quantitative analysis of risk from fragmental rockfalls. *Landslides*, *16*(1), 5-21.

Crosta, G. B., & Agliardi, F. (2003). A methodology for physically based rockfall hazard assessment. *Natural Hazards and Earth System Sciences*, *3*(5), 407-422.

Crosta, G. B., & Agliardi, F. (2004). Parametric evaluation of 3D dispersion of rockfall trajectories. *Natural Hazards and Earth System Sciences*, *4*(4), 583-598.

Crosta, G.B.; Agliardi, F.; Frattini, P.; Lari, S. Key Issues in Rock Fall Modeling, Hazard and Risk Assessment for Rockfall Protection. In Engineering Geology for Society and Territory—Volume 2; 2015

Crovelli, R. A. (2000). Probability models for estimation of number and costs of landslides. *foot (ft)*, *25*, 0-3048.

Dal Piaz, G. V., Bistacchi, A., Gianotti, F., Monopoli, B., Passeri, L., & Schiavo, A. (2016). Note illustrative del F. 070 Monte Cervino della Carta Geologica d'Italia alla scala 1: 50.000.

Dattola, G., Crosta, G. B., & di Prisco, C. (2021). Investigating the influence of block rotation and shape on the impact process. *International Journal of Rock Mechanics and Mining Sciences*, *147*, 104867.

Dorren, L. K. A., Berger, F., & Putters, U. S. (2006). Real-size experiments and 3-D simulation of rockfall on forested and non-forested slopes. *Natural hazards and earth system sciences*, *6*(1), 145-153.

Dorren, L.K.A., Berger, F., Imeson, A.C., Maier, B. & Rey, F. 2004a. Integrity, stability and management of protection forests in the European Alps. Forest Ecology and Management 195: 165-176.

Dorren, L.K.A., Maier, B., Putters, U.S. & Seijmonsbergen, A.C. 2004b. Combining field and modelling techniques to assess rockfall dynamics on a protection forest hillslope in the European Alps. Geomorphology 57: 151-167.

Dupire, S., Bourrier, F., Monnet, J. M., Bigot, S., Borgniet, L., Berger, F., & Curt, T. (2016). Novel quantitative indicators to characterize the protective effect of mountain forests against rockfall. *Ecological Indicators*, *67*, 98-107.

Dussauge-Peisser, C., Helmstetter, A., Grasso, J. R., Hantz, D., Desvarreux, P., Jeannin, M., & Giraud, A. (2002). Probabilistic approach to rock fall hazard assessment: potential of historical data analysis. *Natural hazards and earth system sciences*, *2*(1/2), 15-26.

Evans, S. G., & Hungr, O. (1993). The assessment of rockfall hazard at the base of talus slopes. *Canadian geotechnical journal*, *30*(4), 620-636.

Farvacque, M., Eckert, N., Bourrier, F., Corona, C., Lopez-Saez, J., & Toe, D. (2021). Quantile-based individual risk measures for rockfall-prone areas. International Journal of Disaster Risk Reduction, 53, 101932.

Farvacque, M., Lopez-Saez, J., Corona, C., Toe, D., Bourrier, F., & Eckert, N. (2019). Quantitative risk assessment in a rockfall-prone area: the case study of the Crolles municipality (Massif de la Chartreuse, French Alps). Géomorphologie: relief, processus, environnement, 25(1), 7-19.

Frattini, P., Crosta, G. B., Agliardi, F., Clague, J. J., & Stead, D. (2012). 22 Rockfall characterization and modeling. *Landslides: types, mechanisms and modeling*, 267.

Getzner M, Gutheil-KnoppKirchwald G, Kreimer E, Kirchmeir H, Huber M. Gravitational natural hazards: Valuing the protective function of alpine forests. Forest Policy and Economics, 2017;80: 150-159.

Grêt-Regamey A, Bebi P, Bishop, ID, Smid WA. Linking GIS-based models to value ecosystem services in an alpine region. Journal of Environmental Management, 2008. 89(3);197-208.

Guccione, D. E., Giacomini, A., Thoeni, K., Fityus, S., & Buzzi, O. (2022). On the Dynamic Fragmentation of Rock-Like Spheres: Insights into Fragment Distribution and Energy Partition. *Rock Mechanics and Rock Engineering*, 1-27.

Guthrie, R. H., & Evans, S. G. (2004). Magnitude and frequency of landslides triggered by a storm event, Loughborough Inlet, British Columbia. *Natural Hazards and Earth System Sciences*, *4*(3), 475-483.

Guzzetti, F., Reichenbach, P., & Wieczorek, G. F. (2003). Rockfall hazard and risk assessment in the Yosemite Valley, California, USA. *Natural Hazards and Earth System Sciences*, 3(6), 491-503.

Hantz, D., Colas, B., Dewez, T., Lévy, C., Rossetti, J. P., Guerin, A., & Jaboyedoff, M. (2020). Caractérisation quantitative des aléas rocheux de départ diffus. *Revue Française de Géotechnique*, (163), 2.

Hantz, D., Corominas, J., Crosta, G. B., & Jaboyedoff, M. (2021). Definitions and concepts for quantitative rockfall hazard and risk analysis. *Geosciences*, *11*(4), 158.

Hantz, D., Ventroux, Q., Rossetti, J. P., & Berger, F. (2018). A new approach of diffuse rockfall hazard. In Landslides and Engineered Slopes. Experience, Theory and Practice (pp. 1063-1067). CRC Press.

Häyhä T, Franzese P. P, Paletto A, Fath B.D. Assessing, valuing, and mapping ecosystem services in alpine forests. Ecosystem Services, 2015;14:12-24.

Hungr, O., Evans, S. G., & Hazzard, J. (1999). Magnitude and frequency of rock falls and rock slides along the main transportation corridors of southwestern British Columbia. *Canadian Geotechnical Journal*, *36*(2), 224-238.

Jancke, O., Dorren, L. K., Berger, F., Fuhr, M., & Köhl, M. (2009). Implications of coppice stand characteristics on the rockfall protection function. *Forest ecology and management*, *259*(1), 124-131.

Kajdiž, P., Diaci, J., & Rebernik, J. (2015). Modelling facilitates silvicultural decision-making for improving the mitigating effect of beech (Fagus sylvatica L.) dominated alpine forest against rockfall. *Forests*, *6*(6), 2178-2198.

Lambert, S., Toe, D., Mentani, A., & Bourrier, F. (2021). A meta-model-based procedure for quantifying the on-site efficiency of rockfall barriers. Rock Mechanics and Rock Engineering, 54(2), 487-500.

Lari, S., Frattini, P., & Crosta, G. B. (2014). A probabilistic approach for landslide hazard analysis. *Engineering geology*, *182*, 3-14.

Leine, R. I., Schweizer, A., Christen, M., Glover, J., Bartelt, P., & Gerber, W. (2014). Simulation of rockfall trajectories with consideration of rock shape. *Multibody System Dynamics*, *32*(2), 241-271.

Macciotta, R., Martin, C. D., & Cruden, D. M. (2015). Probabilistic estimation of rockfall height and kinetic energy based on a three-dimensional trajectory model and Monte Carlo simulation. Landslides, 12(4), 757-772.

Malamud, B. D., Turcotte, D. L., Guzzetti, F., & Reichenbach, P. (2004). Landslide inventories and their statistical properties. *Earth Surface Processes and Landforms*, *29*(6), 687-711.

Matas, G.; Lantada, N.; Corominas, J.; Gili, J. A.; Ruiz-Carulla, R.; Prades, A., RockGIS: a GIS-based model for the analysis of fragmentation in rockfalls. *Landslides 2017*, 14 (5), 1565-1578.

565   Matasci, B., Jaboyedoff, M., Loye, A., Pedrazzini, A., Derron, M. H., & Pedrozzi, G. (2015). Impacts of fracturing patterns on the rockfall susceptibility and erosion rate of stratified limestone. Geomorphology, 241, 83-97.

Melzner, S., Rossi, M., & Guzzetti, F. (2020). Impact of mapping strategies on rockfall frequency-size distributions. *Engineering Geology*, *272*, 105639.

570   Moos C, Bebi P, Schwarz M, Stoffel M, Sudmeier-Rieux K, Dorren L. Ecosystem-based disaster risk reduction in mountains. Earth-Science Reviews, 2018;177: 497-513.

Moos, C. A., & Dorren, L. (2021). Cost-benefit analysis as a basis for risk-based rockfall protection forest management.

Moos, C., Fehlmann, M., Trappmann, D., Stoffel, M., & Dorren, L. (2018). Integrating the mitigating effect of forests into quantitative rockfall risk analysis–Two case studies in Switzerland. *International journal of disaster risk reduction*, *32*, 55-74.

575   Nocilla, N., Evangelista, A., & Di Santolo, A. S. (2009). Fragmentation during rock falls: two Italian case studies of hard and soft rocks. Rock mechanics and rock engineering, 42(5), 815.

Perret, S., Dolf, F., & Kienholz, H. (2004). Rockfalls into forests: analysis and simulation of rockfall trajectories— considerations with respect to mountainous forests in Switzerland. *Landslides*, *1*(2), 123-130.

Pfeiffer, T.J., and Bowen, T.D., "Computer Simulation of Rockfalls." Bulletin of Association of Engineering Geologists.
580   Vol. 26, No. 1. 1989. pp135-146

Polino, R., Bonetto, F., Carraro, F., Gianotti, F., Gouffon, Y., Malusà, M. G., ... & Schiavo, A. (2015). Foglio 090 Aosta della Carta Geologica d'Italia.

Radtke, A., Toe, D., Berger, F., Zerbe, S., & Bourrier, F. (2014). Managing coppice forests for rockfall protection: lessons from modeling. *Annals of Forest Science*, *71*(4), 485-494.

585   Rammer, W., Brauner, M., Dorren, L. K. A., Berger, F., & Lexer, M. J. (2010). Evaluation of a 3-D rockfall module within a forest patch model. *Natural Hazards and Earth System Sciences*, *10*(4), 699-711.

Rosser, N., Lim, M., Petley, D., Dunning, S., & Allison, R. (2007). Patterns of precursory rockfall prior to slope failure. Journal of geophysical research: earth surface, 112(F4).

Ruiz Carulla, R. (2018). Rockfall analysis: failure, fragmentation and propagation characterization: a fractal fragmentation
590   of rockfalls.

Ruiz-Carulla, R., Corominas, J., & Mavrouli, O. (2017). A fractal fragmentation model for rockfalls. *Landslides*, *14*(3), 875-889.

Shen, W. G., Zhao, T., Crosta, G. B., & Dai, F. (2017). Analysis of impact-induced rock fragmentation using a discrete element approach. *International Journal of Rock Mechanics and Mining Sciences*, 98, 33-38.
595

Stoffel, M., Wehrli, A., Kühne, R., Dorren, L. K., Perret, S., & Kienholz, H. (2006). Assessing the protective effect of mountain forests against rockfall using a 3D simulation model. *Forest Ecology and Management*, *225*(1-3), 113-122.

Toe, D., Bourrier, F., Dorren, L., & Berger, F. (2018). A novel DEM approach to simulate block propagation on forested slopes. *Rock Mechanics and Rock Engineering*, *51*(3), 811-825.

600 UNI (2012) UNI 112111-4: 2012 rockfall protective measures – Part 4: definitive and executive design. Ente Nazionale Italiano di Unificazione, Milano Italia (in Italian). ~~http://www.uni.com~~http://www.uni.com

Volkwein, A., Roth, A., Gerber, W., & Vogel, A. (2009). Flexible rockfall barriers subjected to extreme loads. *Structural engineering international*, *19*(3), 327-332.

Volkwein, A., Schellenberg, K., Labiouse, V., Agliardi, F., Berger, F., Bourrier, F., ... & Jaboyedoff, M. (2011). Rockfall
605 characterisation and structural protection–a review. Natural Hazards and Earth System Sciences, 11(9), 2617-2651.

Yashima S, Kanda Y, Sano S. Relationships between particle size and fracture energy or impact velocity required to fracture as estimated from single particle crushing. Powder Technol. 1987;51: 277–282

Wang, Y., Tonon, F., Crosta, G. B., Agliardi, F., & Zavodni, Z. M. (2010, January). Rock Fragmentation Module in 3-D Rock-fall Analysis. In 44th US Rock Mechanics Symposium and 5th US-Canada Rock Mechanics Symposium. American
610 Rock Mechanics Association
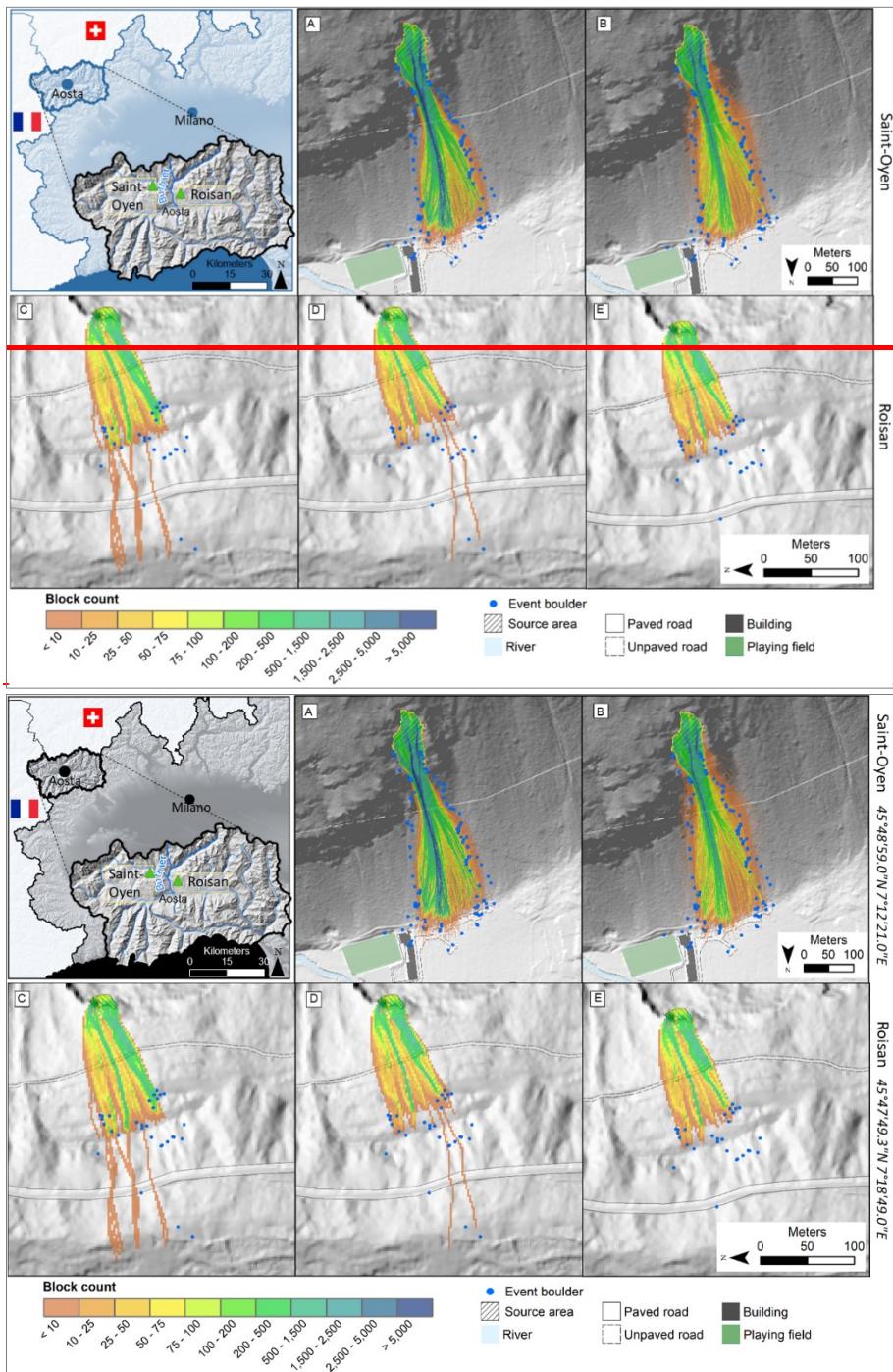
Figure 1 A) Location of the two case studies in Aosta Valley region. The other panels show the back calibration of the rockfall events: A) and B) simulation of Saint-Oyen rockfall (A) with parameters modified to account for the forest (SO_HS) and (B) by adopting the Hy-Stone tree-impact algorithm (SO_HS_tree); C) and D) simulation of Roisan rockfall (C) with parameters

modified to implicitly account for the possibility of fragmentation (R_HS) and (D) by adopting the Hy-Stone fragmentation algorithm (R_HS$_{frag}$). Panel E) shows the calibration R_HS$_{short}$, obtained by neglecting the most distal blocks: this approach simulates only the blocks that stopped in the main deposit, without crossing the paved road.

620
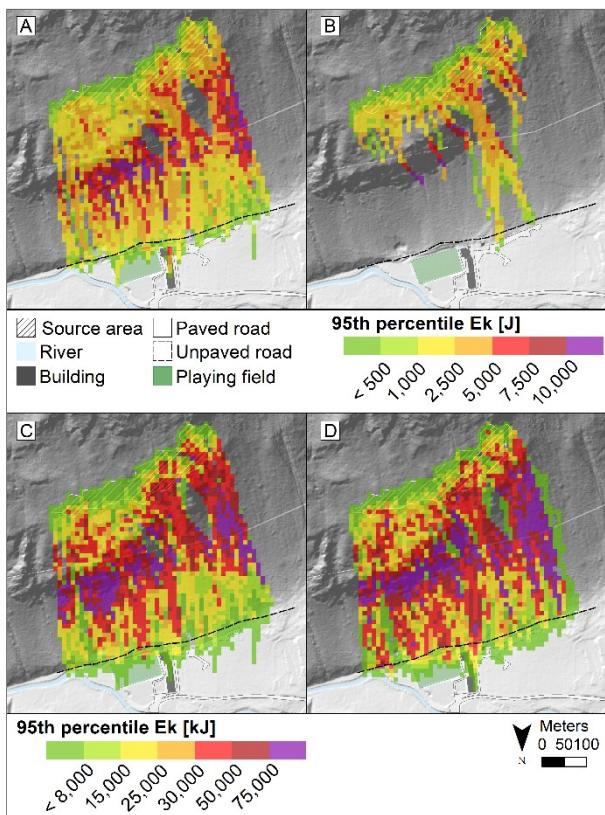
Figure 2 Distribution of kinetic energies of blocks along the slope in Saint-Oyen case study. The value of each cell corresponds to the 95th percentile of the kinetic energy of the blocks passing through that cell. Box A) scenario S1 (small blocks) HS, B) scenario S1 (small blocks) HS$_{tree}$, C) scenario S5 (large blocks) HS, D) scenario S5 HS$_{tree}$ (large blocks).

625
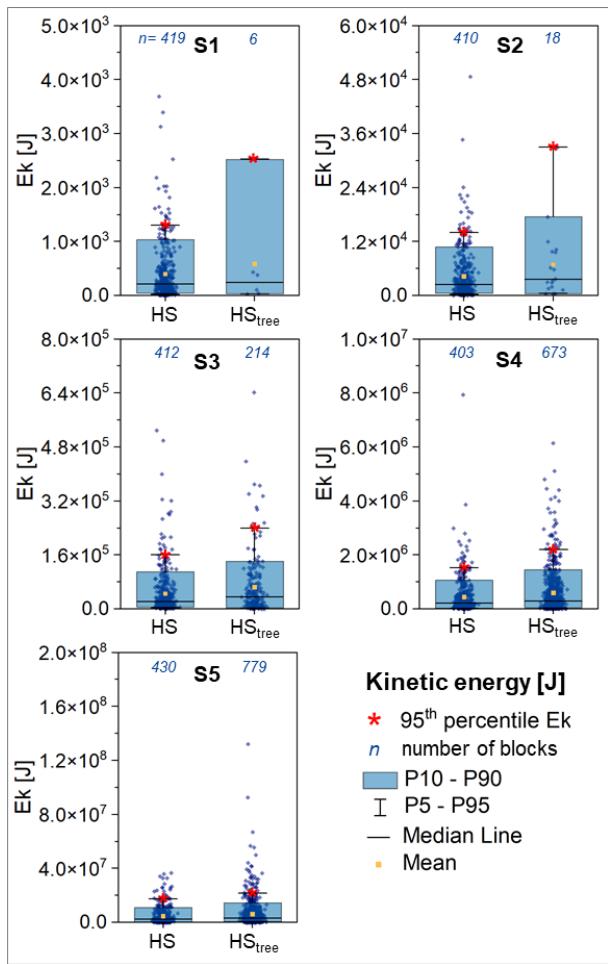
Figure 3 Boxplots of kinetic energy values recorded for each scenario (S1 to S5) at the foot of the slope in Saint-Oyen case study. The associated 95th percentile value is highlighted by the red star. The total number of simulated blocks for each scenario is 995.

630
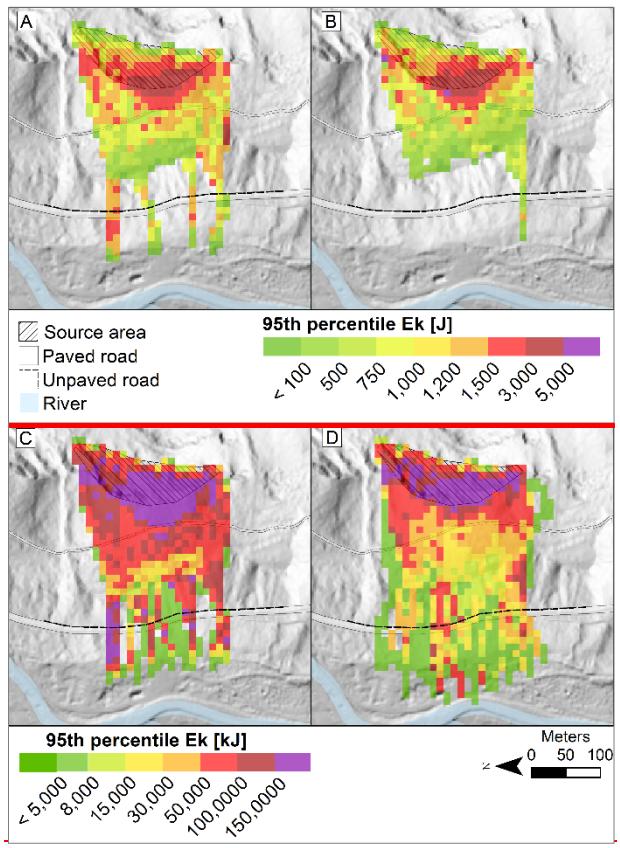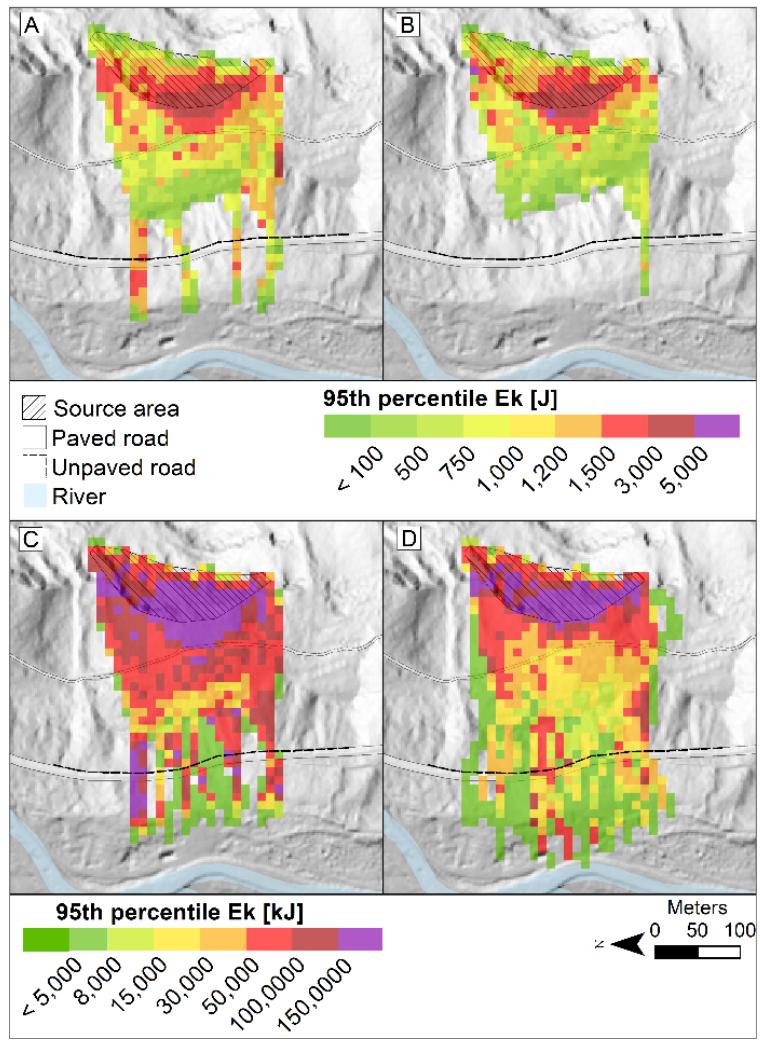
Figure 4 Distribution of kinetic energy of blocks along the slope in Roisan case study. The value of each cell corresponds to the 95th percentile of the kinetic energy of the blocks passing through that cell. Box A) scenario S1 (small blocks) HS, B) scenario S1 (small blocks) HSfrag, C) scenario S5 (large blocks) HS, D) scenario S5 (large blocks) HSfrag.
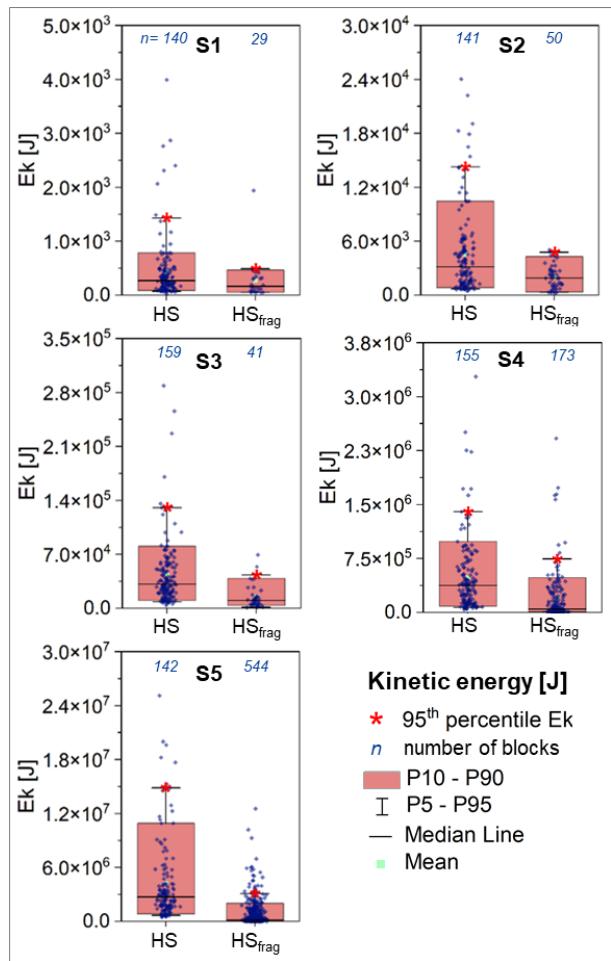
Figure 5 Boxplots of kinetic energy values recorded along the road at the foot of the slope in Roisan case study. The associated 95th percentile value is highlighted by the red star. The total number of simulated blocks is 2646.
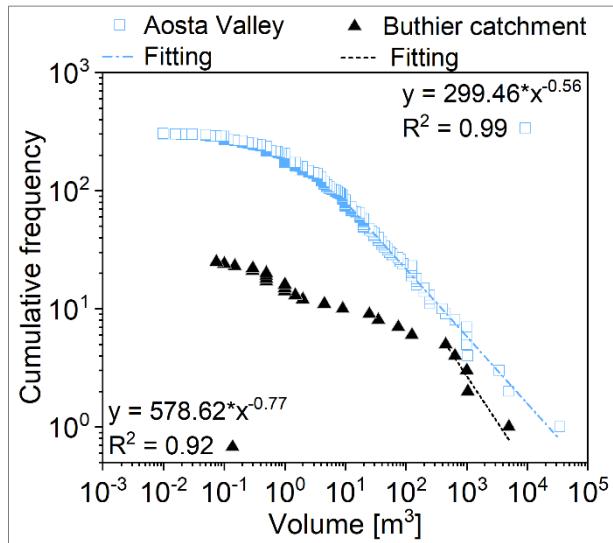
Figure 6 The two magnitude frequency relationships of 306 rockfall events collected in the Aosta Valley region (blue empty squares) and the 25 events from the Buthier catchment (black triangles).
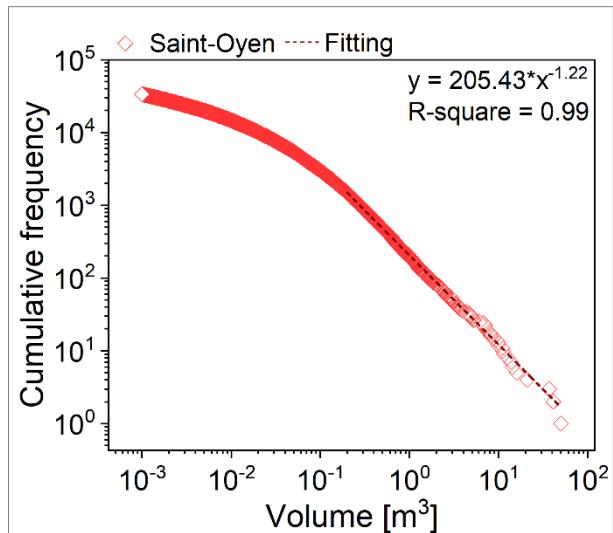
Figure 7 The size frequency relationship of blocks along the talus obtained by image analysis for the Saint-Oyen event.

650
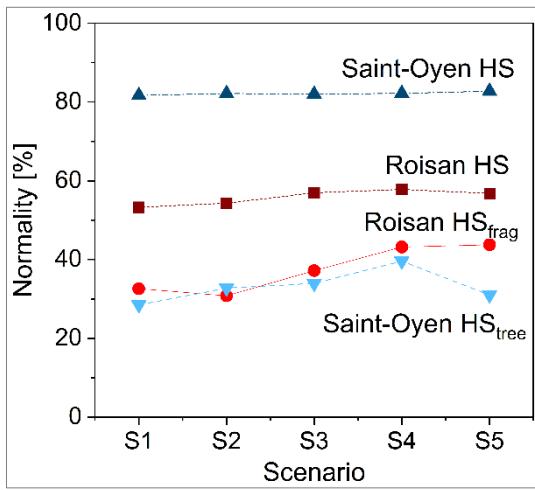
Figure 8 Test of the normality of log-kinetic energy distribution within 10x10 m cells for all the volume scenarios. The y-axis shows the percentage of cells where the normality is not rejected by the Kolmogorov-Smirnov test.
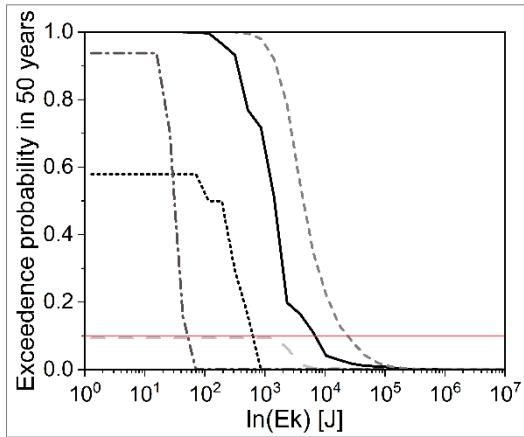
655   *Figure 9 Example of hazard curves characterized by a non-logarithmic trend, calculated in five cells of R_HS model.*
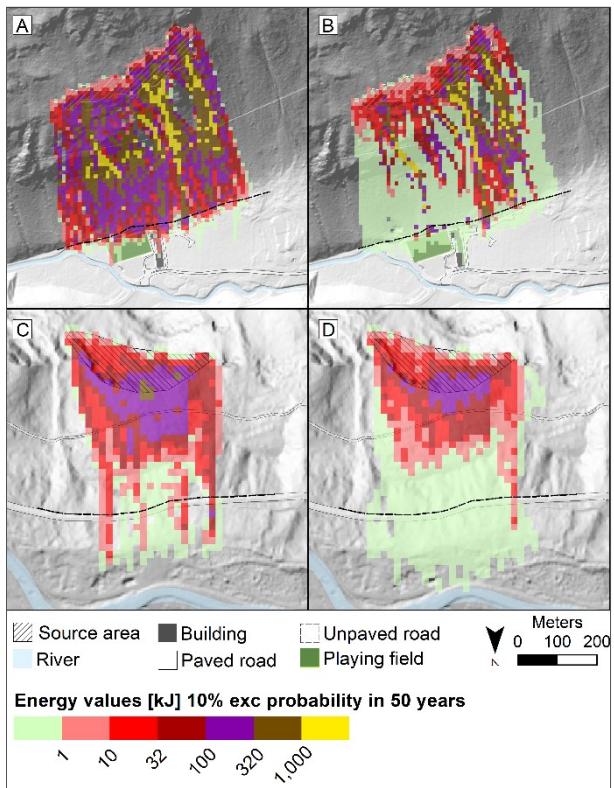
Figure 10 Hazard map for: A) Saint-Oyen SO_HS model, B) Saint-Oyen SO_HS$_{tree}$ model, C) Roisan R_HS model, and D) Roisan R_HS$_{frag}$ model. The hazard is quantified as the kinetic energy associated to a 10% probability in 50 years.

660
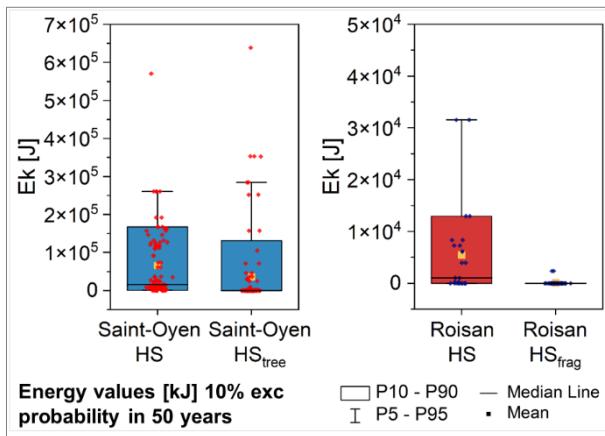
Figure 11 Boxplot of the kinetic energy associated to a 10% probability in 50 years for Saint-Oyen (blue boxplots on the left) and Roisan (red boxplots on the right) case studies, recorded along the road at the foot of the slope (dashed line in Figure 10).

665 *Table 1 Values of normal (e_n) and tangential restitution (e_t) coefficients and of the friction coefficient (μ_s) for the different slope materials used in the rockfall numerical simulations for the Saint-Oyen case study.*

Material	e_n [-]	e_t [-]	μ_s [-]
Outcropping rock	85	85	0.3
Coarse bare debris	65	70	0.55
Fine bare debris	55	65	0.45
Slope debris + damaged forest[1]	64	71	0.5
Slope debris + undamaged forest[1]	75	80	0.4
Alluvial deposit	55	74	0.4
Paved road	70	77	0.3
Unpaved road	60	70	0.3
Buildings	20	10	1

[1] *Only for the explicit approach (HStree)*

Table 2 Values of normal (e_n) and tangential restitution (e_t) coefficients and of the friction coefficient (μ_s) for the different
670 *slope materials used in the rockfall numerical simulations for the Roisan case study.*

Material	e_n [-]	e_t [-]	μ_s [-]
	HS	HS	HS
Outcropping rock	75	85	0.2

Sub-cropping rock	60	70	0.3
Slope debris in HS model	60	65	0.4
Slope debris in HS$_{frag}$ model	50	60	0.5
Paved road	75	85	0.2
Unpaved road	55	65	0.3
Alluvial deposit	40	50	0.35

Table 3 Volume scenarios for hazard analysis.

Scenario	Range of volume [m³]	Roisan – onset frequency f_o	Saint-Oyen – onset frequency f_o
S1	0.001 – 0.01	9	67
S2	0.01 – 0.1	0.6	4.0
S3	0.1 - 1	0.03	0.24
S4	01-10	0.002	0.015
S5	10 -100	0.0001	0.0009

675